High-pressure phase diagram of $NdFeAsO_{0.9}F_{0.1}$: Disappearance of superconductivity on the verge of ferromagnetism from Nd moments

M. Abdel-Hafiez,[1,2,3,*] M. Mito,[4] K. Shibayama,[4] S. Takagi,[4] M. Ishizuka,[5] A. N. Vasiliev,[3,6,7] C. Krellner,[2] and H. K. Mao[1]

[1]*Center for High Pressure Science and Technology Advanced Research, Beijing, 100094, China*

[2]*Institute of Physics, Goethe University Frankfurt, D-60438 Frankfurt/M, Germany*

[3]*National University of Science and Technology (MISiS), Moscow 119049, Russia*

[4]*Graduate School of Engneering, Kyushu Institute of Technology, Fukuoka 804-8550, Japan*

[5]*Renovation Center of Instruments for Science Education and Technology, Osaka University, Osaka 560-0043, Japan*

[6]*Moscow State University, Moscow 119991, Russia*

[7]*National Research South Ural State University, Chelyabinsk 454080, Russia*

(Received 22 January 2018; revised manuscript received 1 July 2018; published 4 September 2018)

We investigated transport and magnetic properties of single crystal $NdFeAsO_{0.9}F_{0.1}$ under hydrostatic pressures up to 50 GPa. The ambient pressure superconductivity at $T_c \sim 45.4$ K was fully suppressed at $P_c \sim 21$ GPa. Upon a further increase of pressure, ferromagnetism associated with the order of the rare-earth subsystem was induced at the border of superconductivity. Our finding is supported by the hysteresis in the magnetization $M(H)$ loops and the strong increase in the field cooled data $M(T)$ toward low temperatures. We also show that the temperature evolution of the electrical resistivity as a function of pressure is consistent with a crossover from a Fermi liquid to non-Fermi liquid to Fermi liquid. The Hall measurements suggest that the multiband electronic structures have changed with pressure, which should also affect the resistivity behavior. These results give access to the high-pressure side of the superconducting phase diagram in the 1111 type of materials.

DOI: 10.1103/PhysRevB.98.094504

I. INTRODUCTION

A key topic in current research of strongly correlated heavy fermion systems, high-T_c cuprates, and ferrates is the coexistence and competition between superconductivity and various electronic orders [1–3]. In conventional superconductors, the electron-phonon interaction gives rise to the attraction between electrons with opposite momenta and opposite spins. This causes superconductivity characterized by spin-singlet *s*-wave Cooper pairing and conservation of the time-reversal symmetry [4]. In contrast, ferromagnetism breaks the time reversal symmetry, which makes these two phenomena antagonistic to each other. There are systems, however, where both superconductivity and ferromagnetism stems from the same electrons, although magnetism is suppressed prior to the emergent superconducting (SC) order. In the heavy fermion compounds UGe_2[5] and URhGe [6,7] superconductivity on the verge of ferromagnetism is understood by magnetic interactions which presumes that spin-triplet pairing is advantageous to the spin-singlet pairing. An antiferromagnetism is not excluded by superconductivity since the average values of the magnetic induction and exchange field are negligibly small on the scale of the SC correlation length [8]. A unique coexistence of superconductivity, antiferromagnetism, and ferromagnetism was observed in $RuSr_2GdCu_2O_8$, where all these phenomena were attributed to spatially separated CuO_2 planes, and Gd and Ru magnetic moments [9]. Similarly, the coexistence of spatially separated ferromagnetism and superconductivity was observed in the ferroarsenite family [9–11]. The systems that evidence not just the coexistence but also the interplay of these quantum cooperative phenomena in a single material are the most interesting.

The normal state of high-T_c superconductors is quite unusual. The electrical resistivity varies with temperature in a peculiar way which deviates significantly from $\sim T^2$ dependence expected from the Fermi-liquid (FL) theory of metals [12–15]. Since non-Fermi-liquid (NFL) behavior is often seen above a SC dome, there is a consensus that its origin may hold the key to understand the pairing mechanism in high-T_c superconductors [15]. Studies on the high-T_c cuprates [9,13,14], heavy fermion metals [15], organic Bechgaard salts [16], and iron-based superconductors [17–20] imply that NFL behavior and high-T_c SC dome favor proximity to magnetic order. This fact has led to proposals ascribing both NFL behavior and high-T_c superconductivity to spin fluctuations close to a magnetic quantum critical point [21,22]. At present, the microscopic mechanism of the NFL behavior and its relationship to high-T_c superconductivity are still under considerable debate.

The 1111-type iron-based superconductors $LnFeAsO_{1-x}F_x$ (Ln stands for lanthanide) were the first material with a T_c above 50 K, besides the cuprate superconductors [23]. A change of the rare-earth ion or application of high pressure to the 1111-type materials [24–27] has revealed the substantial influence of the interionic distances on the T_c. Thus, finding a way to tune the physical properties of $NdFeAsO_{0.9}F_{0.1}$ is important not only for understanding all of these interesting features but also for exploring the underlying mechanism of superconductivity in the iron-based superconductors. Hydrostatic pressure

*mahmoudhafiez@gmail.com

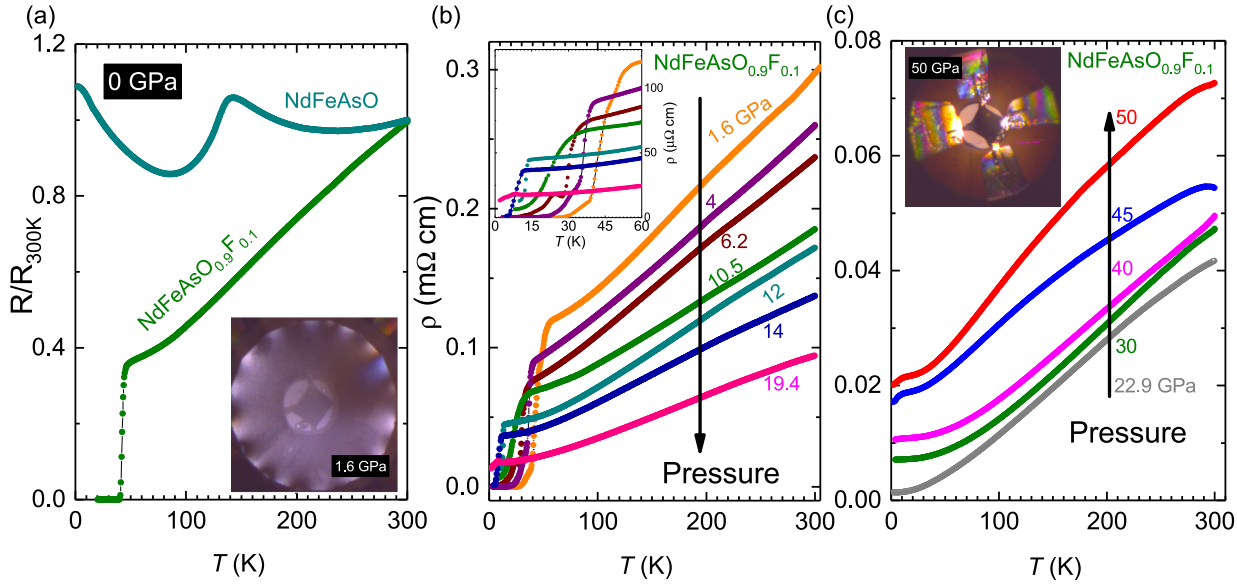

FIG. 1. (a) The T dependence of the in-plane resistance measurements upon heating the $NdFeAsO_{1-x}F_x$ single crystals at $x = 0$ and 0.1. (b) In-plane electrical resistivity ρ versus temperature between 1.6 and 19.4 GPa. The inset is a closeup of the low-temperature region, highlighting the SC transition. (c) The T dependence of the resistivity curves at pressures between 22.9 and 50 GPa. The insets of (a) and (c) images of the $NdFeAsO_{0.9}F_{0.1}$ sample mounted in a diamond anvil cell at 1.6 and 50 GPa, respectively.

is a tool widely used to study materials without changing their stoichiometry [28–30]. A number of important results have been obtained for iron-based superconductors using high-pressure techniques [27,31–37]. Up to date, the suppression of superconductivity under pressure in the 1111 type of materials is not well studied.

To this end, we performed transport and magnetic property studies on a $NdFeAsO_{0.9}F_{0.1}$ single crystal under hydrostatic pressures up to 50 GPa. Relatively few studies on $NdFeAsO_{0.9}F_{0.1}$ have been published so far. The reason for this poor understanding of superconductivity is that the current Nd1111 system phase diagrams (T_c vs F content) were obtained from polycrystals [38,39], which are problematic due to (foreign phases, local variation of the F content, etc.). We find that while superconductivity is monotonically suppressed with increasing the pressure, the transport properties reveal a prominent FL-NFL-FL crossover. We construct the most comprehensive unique pressure-temperature phase diagram mapping out the explicit evolutions with pressure. Our observations provide upon further increasing pressure a clear evidence of ferromagnetism which arises from the $4f$ moments due to Nd. Our results highlight a competing nature between magnetic order and high-T_c superconductivity in the phase diagram of $NdFeAsO_{0.9}F_{0.1}$, which is a key material among the iron-based superconductors. The paper is organized as follows. In Sec. II we give technical details of experimental techniques. Experimental results are presented in Sec. III. In Secs. IV and VI discussions and conclusions will be presented.

II. MEASUREMENT TECHNIQUES

High-quality single crystals of NdFeAsO and fluorine-doped NdFeAsO were grown out of NaCl/KCl flux at ambient pressure as a new method [40]. Due to the toxicity of arsenic, all procedures related to the sample preparation were performed in a glove box. Starting materials were pristine Neodymium and arsenic as well as iron(III)-oxide powder and iron(II)-fluoride powder. After mixing together the educts were transferred into a glassy carbon crucible. As flux material an eutectic mixture of NaCl and KCl was used, with a molar material to flux ratio of 1:7. Batches with platletlike single crystals were carefully examined by electron probe microanalyzer and x-ray powder diffraction. Further details of the characterization and growth can be found in [40].

A nonmagnetic diamond anvil cell (DAC) was used for high-pressure resistivity measurements. Four contacts were used to measure the high-pressure in-plane resistivity with the superconductor $NdFeAsO_{0.9}F_{0.1}$ set in a diamond anvil cell in the PPMS-9 T (Quantum Design). Single crystals with typical dimensions of $70 \times 70 \times 10\ \mu m^3$ were loaded in sample chambers made by c-BN gasket. We used an insulating gasket made of the mixture of cubic boron nitride with epoxy. Daphne oil 7373 was used as a pressure medium. Pressure was calibrated by using several ruby chips with dimensions of about 1 mm placed into the cell along with the sample at room temperature. Four Pt leads with thickness of about 10 μm and width of about 7–12 μm were used for four-probe measurements. For the magnetic experiments, the dc magnetic susceptibility was observed by the vibrating coil magnetometer using a superconducting quantum interference device magnetometer [41]. The dc field of 30 Oe was applied by the NbTi superconducting magnet. Contraction corresponding to a stress of up to approximately 30 GPa was achieved using a CuBe DAC and combined NiCrAl/CuBe gasket [42]. We used Daphne 7373 oil as a liquidlike pressure-transmitting medium. The pressure value was evaluated measuring the fluorescence of ruby located in the sample cavity. In the

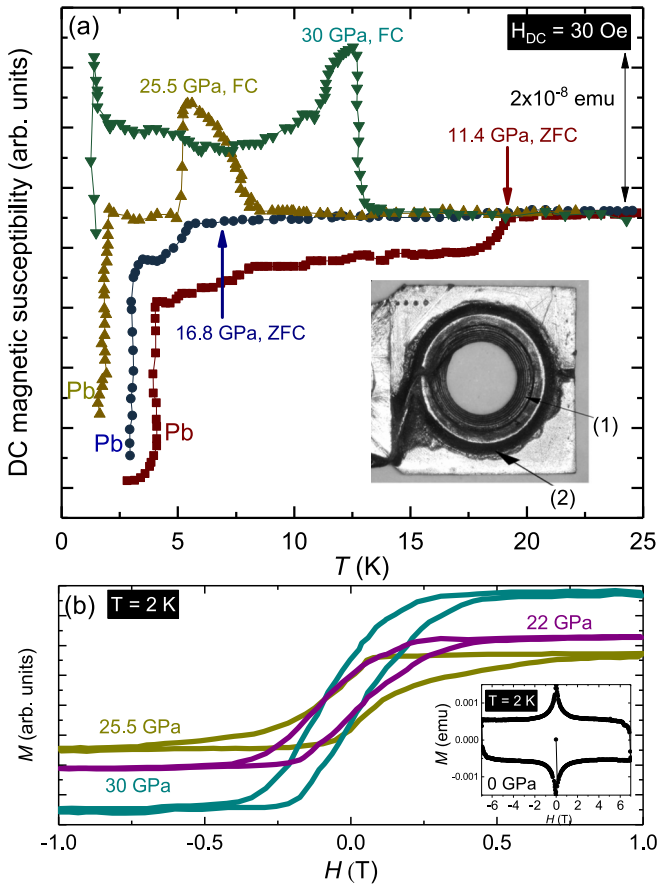

FIG. 2. (a) The temperature dependence of the dc-susceptibility components measured in dc field with an amplitude of 30 Oe. The data were collected upon warming in different dc magnetic fields after cooling in a zero magnetic field. The inset illustrates a photograph of the detection coil. The inside of the main coil [20 turns, marked as (1)] with no bobbin was cone shaped. The compensation coil [20 turns, marked as (2)], covered with Stycast No. 2850FT, was located around the main coil, forming a concentric gradiometer [45]. (b) The magnetic field dependence of the isothermal magnetization M vs H loops were measured at different pressures at 2 K, which is consistent with a standard hysteresis loop for ferromagnets. The inset depicts the magnetic field dependence of the isothermal magnetization M vs H loops measured at 2 K up to 7 T with the field parallel to the c axis.

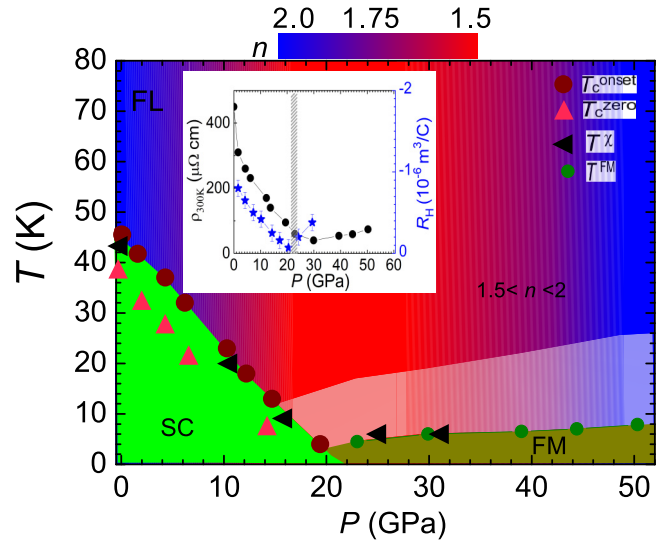

FIG. 3. Pressure-temperature (P-T) phase diagram of $NdFeAsO_{0.9}F_{0.1}$. Pressure dependence of the SC transition temperatures T_cs and a contour color plot of the normal-state resistivity exponent n up to 50 GPa. The temperature dependence of n are extracted from $\rho(T) = \rho_0 + AT^n$ for each pressure. The pink region illustrates that the temperature dependence of n between $1.5 \leqslant n \leqslant 1.75$. The values of T_c^{onset}, T_c^{zero}, T_c^{FM}, and T_c^{χ} were determined from the high-pressure resistivity and dc magnetic susceptibility. Above P_c, local ferromagnetic order from the Nd moments appear, observed in resistivity and susceptibility. The area above the FM regime is obtained from the blue arrows in Figs. 4(i)–4(k). The inset illustrates the pressure dependence of the Hall coefficient R_H, and ρ_{300K}. R_H is extracted from the transverse resistivity ρ_{xy}; see below Fig. 5(c).

sample chamber, lead was also held as the manometer at low temperature as well as the standard sample to judge the sign of magnetization.

III. RESULTS

A. Electrical resistivity and magnetic measurements

Figure 1(a) illustrates the T dependence of the in-plane resistance measurements of NdFeAsO and $NdFeAsO_{0.9}F_{0.1}$ single crystals during heating. In the $NdFeAsO_{0.9}F_{0.1}$ sample, the normal state exhibits simple metallic behavior during cooling down from room T, followed by a sharp SC transition at $T_c \approx 45.4$ K, which agrees with magnetization data [40]. The T_c is monotonically suppressed by increasing pressure up to 19.4 GPa, which can be seen more clearly from the $\rho(T)$ data below 60 K shown in Fig. 1(b). Here, we define the onset T_c^{onset} as the temperature where the $\rho(T)$ starts to deviate from the extrapolated normal-state behavior, and determine T_c^{zero} as the zero-resistivity temperature. The error bars are estimated to be ±1 K. Upon increasing pressure to 19.4 GPa, the T_c^{onset} is gradually suppressed to ∼5 K and the T_c^{zero} can barely be defined down to 2 K, the lowest temperature in this study. The pressure coefficient dT_c/dP is around −2.2 K/GPa. Interestingly, when pressure increased from 22.9 to 50 GPa, T_c was suppressed and a broad transition appeared at low temperatures as shown in Fig. 1(c). A closer inspection of the $\rho(T)$ data in Figs. 1(b) and 1(c) also reveals a gradual evolution of the temperature dependence of normal-state resistivity under pressure.

To clarify the features of the pressure-induced phase transition, we investigated the dc magnetic susceptibility under high pressure. In Fig. 2(a), we show the temperature dependence of the dc-susceptibility components measured in the dc field with an amplitude of 30 Oe. The T dependence of magnetization taken upon warming after field cooling and the pressure was determined by the shift of the SC-T_c of lead located in the gasket hole. We found a significant and rapid increase of the susceptibility with increasing the pressure. The T_c is monotonically suppressed by increasing pressure as shown in the resistivity. This can be seen from the $P = 11.4$ and 16.8 GPa data, in which the Meissner signal was observed

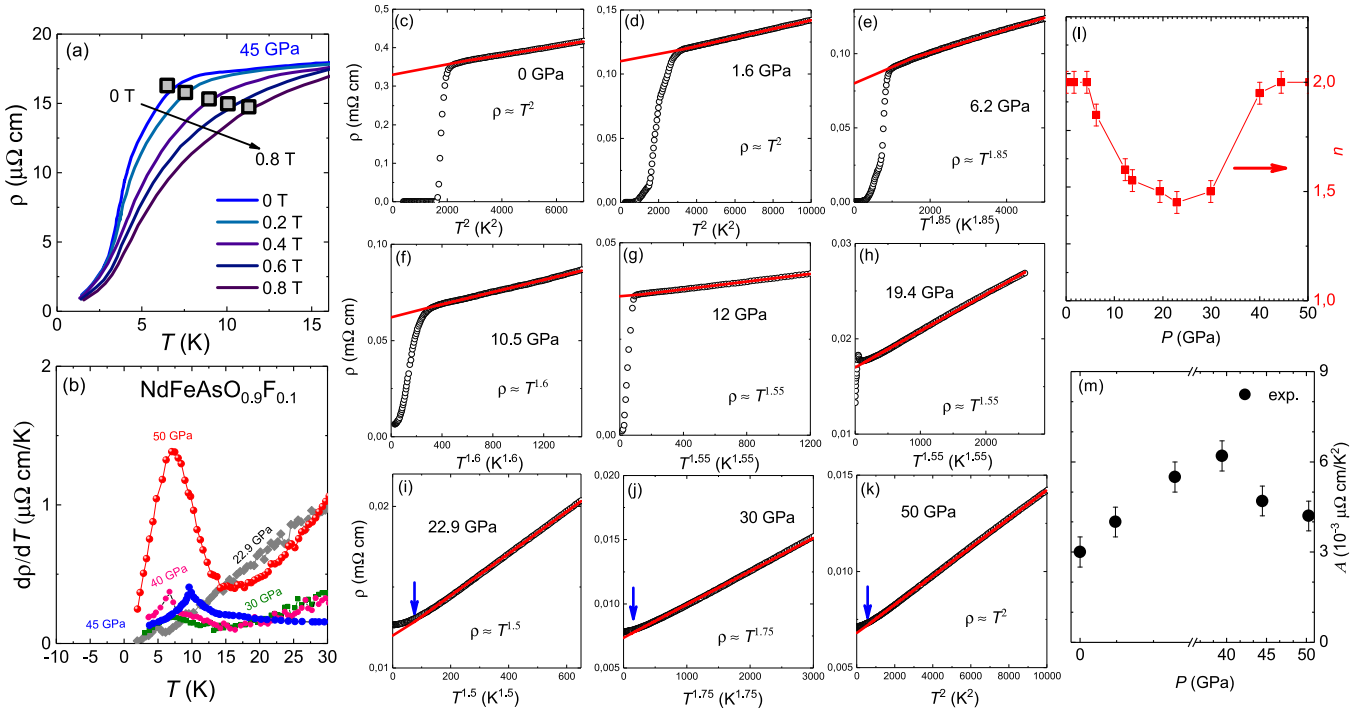

FIG. 4. (a) The resistivity data at different magnetic fields under 45 GPa. The magnetic field broadens the magnetic transition; it also slightly increases the FM transition. (b) T dependence of the derivative of the resistivity $d\rho/dT$ up to 50 Gpa. (c)–(k) Resistivity as a function of T^n for different P values. n is the power determined from the single power-law fit to the resistivity as a function of T presented in (l). The straight solid line in each panel is the linear fit. (m) The parameter A is obtained by fitting the normal state resistivity data below 80 K using this formula: $\rho(T) = \rho_0 + AT^n$.

together with that of lead in the zero-field cooling. Upon further increasing the pressure, at $P = 25.5$ and 30 GPa, the magnetic anomaly is enhanced in the field-cooled scenario upon entering the ferromagnetic phase (FM). In order to confirm this point, we plotted the magnetic field dependence of the isothermal magnetization M vs H loops measured at different pressures at 2 K in Fig. 2(b). The high-pressure behavior for the M vs H loop reveals a magnetic hysteresis loop could be due to the presence of ferromagnetic clusters within spin glass state, which in a way contradicted the existence of long-range magnetic order (of the ferromagnetic or antiferromagnetic type) in this system. While at ambient pressure [inset of Fig. 2(b)], the magnetic hysteresis loop is almost symmetric about the horizontal axis, which indicates that the hysteresis in the crystal arises mainly from bulk flux pinning rather than from the surface barrier. The saturated high-field magnetization increases with increasing pressure, signifying a stabilization of ferromagnetism under pressure.

B. Temperature-pressure phase diagram

The pressure dependencies of the obtained T_c^{onset}, T_c^{zero}, T_c^{FM}, and T_c^{X} for the studied $NdFeAsO_{0.9}F_{0.1}$ are summarized in Fig. 3, which explicitly evidences the gradual suppression of the SC phase followed by the appearance of the FM phase above $P_c \sim 21$ GPa. Upon lowering the temperature, $\rho(T)$ displays a broad anomaly which reflects the onset of ferromagnetic ordering. The evolution of this anomaly under pressure can be clearly seen in the derivative of the high-pressure data illustrated in Fig. 4(b). The nature of this magnetic transition is ferromagnetic, as shown by the T dependence of the in-plane resistivity at different magnetic fields at 45 GPa [see Fig. 4(a)], which show that the magnetic field broadens and slightly increases the magnetic transition. A square represents the transition temperature for each field calculated from the higher temperature peak of the derivative $d\rho/dT$. Such an evolution of the SC and FM phases is observed in other Fe-based superconductors [43,44]. Since the Ruderman-Kittel-Kasuya-Yosida (RKKY) exchange coupling between the Nd local moments is oscillatory with distance, starting with FM coupling at low distances, the general trend towards ferromagnetism under pressure is expected [43]. Interestingly, recent studies using a minimal multiband model, have shown that the Fermi surface nesting has a strong influence on the RKKY interaction [43,46]. In $CeFeAsO_{1-x}F_x$ the suppression of the AFM ordering alone is not sufficient for the emergence of Ce-FM ordering as shown by F-doping studies [47]. Therefore, the origin for this behavior is more complex than a possible simple sign change of the RKKY interaction [48].

C. Fermi liquid to non-Fermi liquid

To gain insights into the peculiar non-Fermi-liquid behavior, we measured the magnetic field dependence of Hall resistivity $[\rho_{xy}(H)]$ at different pressure. We noticed that all curves in Fig. 5(c) have sublinearity versus the magnetic field. Upon increasing pressure, all curves exhibit a negative slope in the whole investigated magnetic-field range. The inset of Fig. 3 presents the pressure dependence of the Hall coefficient, defined as the field derivative of $\rho_{xy}(H)$, $R_H \equiv \rho_{xy}(H)/dH$,

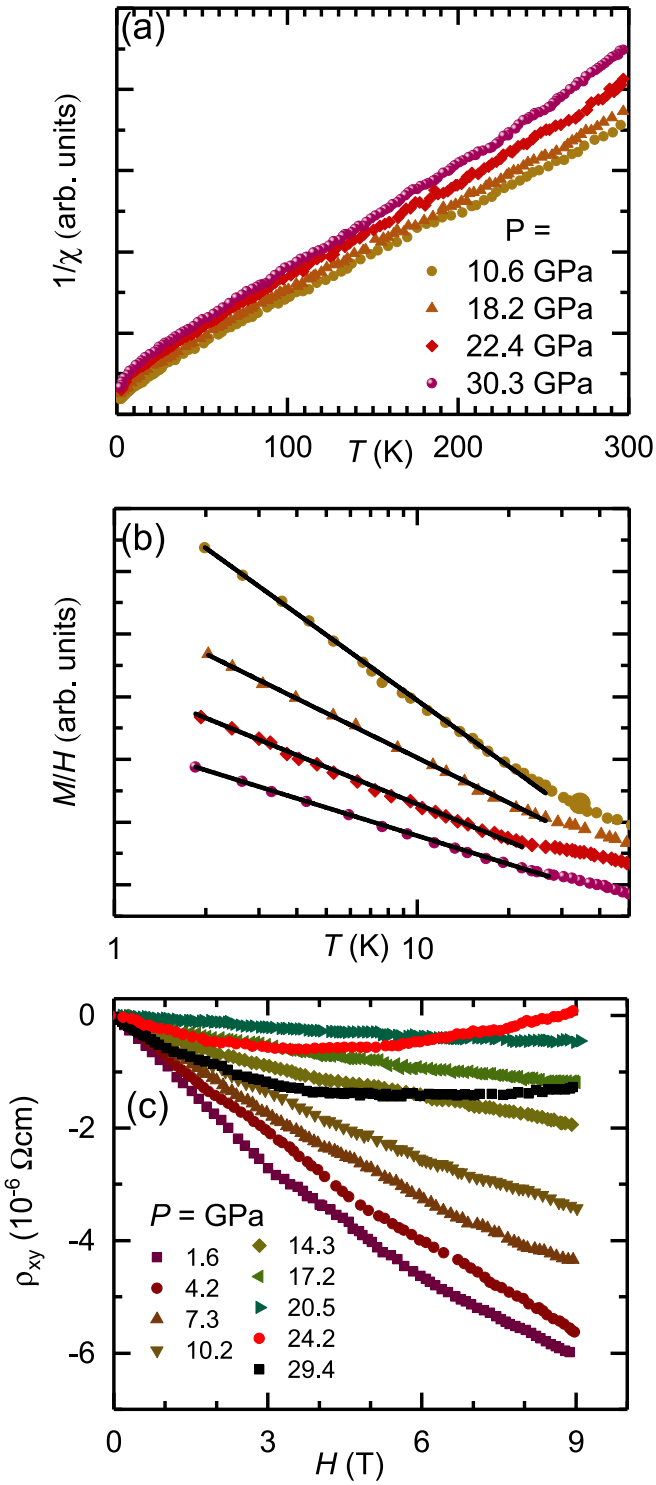

FIG. 5. (a) Zero-field cooled at 10 KOe presents the temperature-dependent inverse magnetic susceptibility. (b) Semilogarithmic plot of the low-temperature susceptibility. Black lines are the linear fit as follows: $M/H \sim \log_{10} T$, which illustrates signature non-Fermi-liquid behavior. The data are shifted vertically for clarity. (c) The field dependence of Hall resistivity $\rho_{xy}(H)$ of the $NdFeAsO_{0.9}F_{0.1}$ single crystal at pressures up to 20.5 GPa at 60 K. Hall coefficient R_H extracted from the transverse resistivity ρ_{xy}. The pressure dependence of the Hall coefficient, defined as the field derivative of $\rho_{xy}(H)$, $R_H \sim \rho_{xy}(H)/dH$, as the slope of a linear fitting to $\rho_{xy}(H)$ is presented in the inset of Fig. 3.

as the slope of a linear fitting to $\rho_{xy}(H)$. In fact, the negative sign of R_H is clearly in the whole pressure range, suggesting that the electron-type carriers dominate the charge transport in the $NdFeAsO_{0.9}F_{0.1}$ system. R_H is negative, and its magnitude first increases slightly with pressure and then experiences a quick reduction above 20 GPa. Such a significant change in the pressure dependence of R_H reflects a pronounced change in the band structure of $NdFeAsO_{0.9}F_{0.1}$ under pressure. The emergence of FM and the change of the R_H -pressure dependence at the same pressure indicate a close connection between them. Additionally, we noticed that both R_H and T_c show similar pressure dependence behavior. Furthermore, we performed a high-pressure magnetic susceptibility at 10 KOe measured between 10 and 30 GPa, in order to uncover the origin of such an intriguing phenomenon. We plotted the temperature-dependent inverse magnetic susceptibility under several pressures; see Fig. 5(a). Additionally, we show a semilogarithmic plot of low-temperature susceptibility in Fig. 5(b). The data are shifted slightly vertically for more clarity and follow $M/H \sim \log_{10} T$, which illustrates signature non-Fermi-liquid behavior [49]. However, the microscopic origin of the NFL behavior is still under debate in several materials. In general, careful analysis of Fe-based compounds will help to investigate the validity of pro-posed theories and, perhaps, provide a unifying model for the breakdown of Fermi-liquid theory in all classes of the Fe-based materials.

IV. DISCUSSION

The Hall measurements suggest that the multiband electronic structures have changed with pressure, which should also affect the resistivity behavior. To uncover the origin of this crossover from Fermi-liquid to non-Fermi-liquid behavior under pressure, we investigated the normal-state properties, which are usually tightly correlated with the SC states for unconventional superconductors. Figure 1(b) shows a distinct change in the temperature dependence of normal-state resistivity already. To quantify this evolution, we fit the $\rho(T)$ to a single power law $\rho(T) = \rho_0 + AT^n$, [see Figs. 4(c)–4(k)], in a sliding window width ΔT=20 K, returning the exponent n and the residual resistivity ρ_0. The power law analysis was done way above the T_c and magnetic order. The evolution of n with doping is summarized in Fig. 4(l). In $NdFeAsO_{0.9}F_{0.1}$ (from 0 to 4 GPa), the exponent n is 2 below 100 K, i.e., the resistivity varies quadratically with temperature, indicating a FL normal state. Upon further pressure increase, n decreases, reaching a minimum of 1.5 at $P = 14$ GPa. n begins to increase and recovers to a value of 2 again at about $P = 40$ GPa. The minimum of n near $P_c = 21$ GPa might be related to a change of the electronic structure. These results of n illustrate that a pressure-induced FL-NFL-FL crossover appears at the high-pressure side of the SC dome in $NdFeAsO_{0.9}F_{0.1}$. This result indicates that the FL-NFL-FL crossover in the investigated system is not tied to the impurity level. Simultaneously, the absolute value of the room temperature resistivity is strongly pressure dependent; see the inset of Fig. 3.

For lightly doped materials, a spin fluctuation resulting from the Fermi surface nesting between hole and electron pockets is a plausible candidate for the pairing mechanism

[25,26,50]. In $NdFeAsO_{0.9}F_{0.1}$, the SDW/structural anomaly is completely suppressed. The normal state exhibits simple metallic behavior upon cooling down from room T, followed by a sharp SC transition at $T_c \approx 45.5$ K of the normal state resistivity. In our results, superconductivity can not be detected above 23 GPa. For the FL behavior, the resistivity ρ is proportional to T^2. However, upon increasing the compression, the resistivity follows $T^{1.5}$ behavior due to the strong quantum fluctuation. This could be a signature of quantum critical point (QCP) [44]. However, all quantum criticality analysis for other systems discussed here was done at low temperatures. In strongly correlated electron systems, the coefficient A of T^2 is often scaled as the strength of the electronic correlations. The sudden change in A reflects the reconstruction of the Fermi surface topology [13]. We found that the parameter A decreases with increasing pressure ($P > 40$ GPa) as shown in Fig. 4(m). If we assumed that the Kadowaki-Woods ratio [51] is maintained under pressure similar to the $BaFe_2(As_{1-x}P_x)_2$ system [19], the parameter A should be proportional to the square of the effective mass m^*. The observed new magnetic ordering in the high compressed $NdFeAsO_{0.9}F_{0.1}$ system indicates the universality of the competition between superconductivity and FM in such a kind of superconducting system [43,44]. It might enhance or drive unconventional superconductivity in iron-based superconductors. The close relationship between the FM and superconductivity indicates the importance of spin fluctuations to mediate superconductivity. Such fluctuations are the leading candidate of the pairing glue in iron-based superconductors. Within the framework of coexistence between superconductivity and FM, one can readily understand why T_c decreases upon applying pressure or doping and eventually approaches absolute zero when the system goes away from it. The decrease of T_c in the doped iron-based compounds when passing through the optimal doping level has been suggested to result from the reduction of the AF spin fluctuations and thus the decrease of m^* [43,44]. In our investigated system, we observed the systematic decrease of T_c and A (thus the square of the effective mass m^*). Finally, it is noteworthy that the temperature dependence of resistivity in the normal state of the overdoped $La_{2-x}Sr_xCuO_4$ shows $T^{1.6}$ at the end of the SC dome, which has been attributed to quantum criticality [13]. Likewise, our observation of similar power-law behavior near the border of the SC dome in the investigated system $NdFeAsO_{0.9}F_{0.1}$ points to plausible common physics that warrants in-depth explorations in the future. Experimentally, these results should stimulate new investigations on $NdFeAsO_{1-x}F_x$ and might also guide explorations of the unconventional origins of the high-T_c superconductivity in this class of materials.

V. CONCLUSIONS

To summarize, through an extensive transport study under high pressure up to 50 GPa, we have clarified in bulk $NdFeAsO_{0.9}F_{0.1}$ the competition between ferromagnetism and superconductivity. FM could be induced by the 4f moments due to Nd upon compression. We construct the pressure-temperature phase diagram which shows a crossover from Fermi liquid to non-Fermi liquid to Fermi liquid (FL-NFL-FL) alongside a monotonic suppression of the superconductivity with increasing the pressure. The phase diagram illustrates that the NFL region is moved to the boundary of the superconducting phase, implying that they are probably governed by different mechanisms. Our results highlight a competing nature between magnetic order and high-T_c superconductivity in the phase diagram of $NdFeAsO_{0.9}F_{0.1}$, and may offer important clues for discussing the unconventional origins of the high-T_c superconductivity in this class of materials. Although, several scenarios have been put forward on the competing origin between electronic order and superconductivity, our results presented here provide an important benchmark for further theoretical work.

ACKNOWLEDGMENTS

We acknowledge Ahuja Rajeef, Roser Valentì, and Ruediger Klingeler for discussions. We are grateful for support from DFG, Deutsche Forschungsgemeinschaft through MO 3014/1-1. This work has been supported by Ministry of Education and Science of Russia through NUST (MISiS) Grant No. K2-2017-084 and by the Act 211 of the Government of Russia, Contract No. 02.A03.21.0004. Grants-in-Aid for Scientific Research, Grants No. (B) 17H03379, from the Ministry of Education, Culture, Sports, Science and Technology (MEXT), Japan.

[1] C. C. Tsuei and J. R. Kirtley, Rev. Mod. Phys. **72**, 969 (2000).
[2] E. Morosan, D. Natelson, A. H. Nevidomskyy, and Q. Si, Adv. Mater. **24**, 4896 (2012).
[3] M. Abdel-Hafiez, Yuanyuan Zhang, Zheng He, Jun Zhao, C. Bergmann, C. Krellner, Chun-Gang Duan, Xingye Lu, H. Luo, P. Dai, and X.-J. Chen, Phys. Rev. B **91**, 024510 (2015).
[4] F. Wang and D. H. Lee, Science **332**, 200 (2011).
[5] S. S. Saxena, K. Ahilan, P. Agarwal, F. M. Grosche, R. K. Haselwimmer, M. Steiner, E. Pugh, I. R. Walker, S. R. Julian, P. Monthoux, G. G. Lonzarich, A. Huxley, I. Sheikin, D. Braithweite, and J. Flouquet, Nature (London) **406**, 587 (2000).
[6] D. Aoki, A. Huxley, E. Ressouche, D. Braithwaite, J. Flouquet, J.-P. Brison, E. Lhotel, and C. Paulsen, Nature (London) **413**, 613 (2001).
[7] D. Braithwaite, D. Aoki, J.-P. Brison, J. Flouquet, G. Knebel, A. Nakamura, and A. Pourret, Phys. Rev. Lett. **120**, 037001 (2018).
[8] L. N. Bulaevskii, A. I. Buzdin, M. L. Kulic, and S. V. Panjukov, Adv. Phys. **34**, 175 (1985).
[9] C. Bernhard, J. L. Tallon, Ch. Niedermayer, Th. Blasius, A. Golnik, E. Brücher, R. K. Kremer, D. R. Noakes, C. E. Stronach, and E. J. Ansaldo, Phys. Rev. B **59**, 14099 (1999).
[10] Z. Ren, Q. Tao, S. Jiang, C. Feng, C. Wang, J. Dai, G. Cao, and Zhu'an Xu, Phys. Rev. Lett. **102**, 137002 (2009).
[11] S. Jiang, H. Xing, G. Xuan, Z. Ren, C. Wang, Z.-a. Xu, and G. Cao, Phys. Rev. B **80**, 184514 (2009).
[12] G. S. Boebinger, Science **323**, 590 (2009).
[13] R. A. Cooper, Y. Wang, B. Vignolle, O. J. Lipscombe, S. M. Hayden, Y. Tanabe, T. Adachi, Y. Koike, M. Nohara, H. Takagi, C. Proust, and N. E. Hussey, Science **323**, 603 (2009).

[14] K. Jin, N. P. Butch, K. Kirshenbaum, J. Paglione, and R. L. Greene, Nature (London) **476**, 73 (2011).

[15] H. V. Löhneysen, A. Rosch, M. Vojta, and P. Wölfle, Rev. Mod. Phys. **79**, 1015 (2007).

[16] N. Doiron-Leyraud, P. Auban-Senzier, S. René dé Cotret, C. Bourbonnais, D. Jérome, K. Bechgaard, and L. Taillefer, Phys. Rev. B **80**, 214531 (2009).

[17] Y. M. Dai, H. Miao, L. Y. Xing, X. C. Wang, P. S. Wang, H. Xiao, T. Qian, P. Richard, X. G. Qiu, W. Yu, C. Q. Jin, Z. Wang, P. D. Johnson, C. C. Homes, and H. Ding, Phys. Rev. X **5**, 031035 (2015).

[18] R. Zhou, Z. Li, J. Yang, D. L. Sun, C. T. Lin, and G.-Q. Zheng, Nat. Commun. **4**, 2265 (2013).

[19] J. G. Analytis, H.-H. Kuo, R. D. McDonald, M. Wartenbe, P. M. C. Rourke, N. E. Hussey, and I. R. Fisher, Nat. Phys. **10**, 194 (2014).

[20] T. Shibauchi, A. Carrington, and Y. Matsuda, Annu. Rev. Condens. Matter Phys. **5**, 113 (2014).

[21] L. Taillefer, Annu. Rev. Condens. Matter Phys. **1**, 51 (2010).

[22] S. Sachdev and B. Keimer, Phys. Today **64**, 29 (2011).

[23] M. Fujioka, S. J. Demholme, T. Ozaki, H. Okazaki, K. Deguchi, S. Demura, H. Hara, T. Watanabe, H. Takeya, T. Yamaguchi, H. Kumakura, and Y. Takano, Supercond. Sci. Technol. **26**, 085023 (2013).

[24] C. de la Cruz, Q. Huang, J. W. Lynn, Jiying Li, W. Ratcliff II, J. L. Zarestky, H. A. Mook, G. F. Chen, J. L. Luo, N. L. Wang, and P. Dai, Nature (London) **453**, 899 (2008).

[25] I. I. Mazin, D. J. Singh, M. D. Johannes, and M. H. Du, Phys. Rev. Lett. **101**, 057003 (2008).

[26] K. Kuroki, S. Onari, R. Arita, H. Usui, Y. Tanaka, H. Kontani, and H. Aoki, Phys. Rev. Lett. **101**, 087004 (2008).

[27] H. Takahashi, K. Igawa, K. Arii, Y. Kamihara, M. Hirano, and H. Hosono, Nature (London) **453**, 376 (2008).

[28] V. Panchal, D. Errandonea, A. Segura, P. Rodriguez Hernandez, A. Munoz, S. Lopez-Moreno, and M. Bettinelli, J. Appl. Phys. **110**, 043723 (2011).

[29] D. Errandonea, E. Bandiello, A. Segura, J. J. Hamlin, Maple, P. Rodriguez-Hernandez, and A. Munoz, J. Alloys Compd. **587**, 14 (2014).

[30] H. K. Mao, B. Chen, J. Chen, K. Li, J.-F. Lin, W. Yang, and H. Zheng, Matter Radiat. Extremes **1**, 59 (2016).

[31] A. Mani, N. Ghosh, S. Paulraj, A. Bharathi, and C. S. Sundar, Europhys. Lett. **87**, 17004 (2009).

[32] F. Ishikawa, N. Eguchi, M. Kodama, K. Fujimaki, M. Einaga, A. Ohmura, A. Nakayama, A. Mitsuda, and Y. Yamada, Phys. Rev. B **79**, 172506 (2009).

[33] E. Colombier, S. L. Bud'ko, N. Ni, and P. C. Canfield, Phys. Rev. B **79**, 224518 (2009).

[34] T. Yamazaki, N. Takeshita, R. Kobayashi, H. Fukazawa, Y. Kohori, K. Kihou, C.-H. Lee, H. Kito, A. Iyo, and H. Eisaki, Phys. Rev. B **81**, 224511 (2010).

[35] S. Medvedev, T. M. McQueen, I. A. Troyan, T. Palasyuk, M. I. Eremets, R. J. Cava, S. Naghavi, F. Casper, V. Ksenofontov, G. Wortmann, and C. Felser, Nat. Mater. **8**, 630 (2009).

[36] L. L. Sun *et al.*, Nature (London) **483**, 67 (2012).

[37] H. Takahashi, H. Soeda, M. Nukii, C. Kawashima, T. Nakanishi, S. Iimura, Y. Muraba, S. Matsuishi, and H. Hosono, Sci. Rep. **5**, 7829 (2015).

[38] G. Lamura, T. Shiroka, P. Bonfà, S. Sanna, R. De Renzi, M. Putti, N. D. Zhigadlo, S. Katrych, R. Khasanov, and J. Karpinski, Phys. Rev. B **91**, 024513 (2015).

[39] L. Malavasi, G. A. Artioli, C. Ritter, M. C. Mozzati, B. Maroni, B. Pahari, and A. Caneschi, J. Am. Chem. Soc. **132**, 2417 (2010).

[40] A. Adamski, C. Krellner, and M. Abdel-Hafiez, Phys. Rev. B **96**, 100503(R) (2017).

[41] M. Ishizuka, M. K. Amaya, and S. Endo, Rev. Sci. Instrum. **66**, 3307 (1995).

[42] M. Ishizuka, Rev. Sci. Instrum. **76**, 123902 (2005).

[43] Y. Tokiwa, S.-H. Hübner, O. Beck, H. S. Jeevan, and P. Gegenwart, Phys. Rev. B **86**, 220505(R) (2012).

[44] A. Jesche, T. Förster, J. Spehling, M. Nicklas, M. de Souza, R. Gumeniuk, H. Luetkens, T. Goltz, C. Krellner, M. Lang, J. Sichelschmidt, H.-H. Klauss, and C. Geibel, Phys. Rev. B **86**, 020501(R) (2012).

[45] M. Ishizuka, H. Manaka, and I. Yamada, J. Phys.: Condens. Matter **18**, 2935 (2006).

[46] A. Akbari, I. Eremin, and P. Thalmeier, Phys. Rev. B **84**, 134513 (2011).

[47] J. Zhao, Q. Huang, C. D. L. Cruz, S. Li, J. W. Lynn, Y. Chen, M. A. Green, G. F. Chen, G. Li, Z. Li, J. L. Luo, N. L. Wang, and P. Dai, Nat. Mater. **7**, 953 (2008).

[48] G. F. Chen, Z. Li, D. Wu, G. Li, W. Z. Hu, J. Dong, P. Zheng, J. L. Luo, and N. L. Wang, Phys. Rev. Lett. **100**, 247002 (2008).

[49] M. B. Maple, M. C. de Andrade, J. Herrmann, Y. Dalichaouch, D. A. Gajewski, C. L. Seaman, R. Chau, R. Movshovich, M. C. Aronson, and R. Osborn, J. Low Temp. Phys. **99**, 223 (1995).

[50] M. Abdel-Hafiez, Y. J. Pu, J. Brisbois, R. Peng, D. L. Feng, D. A. Chareev, A. V. Silhanek, C. Krellner, A. N. Vasiliev, and X.-J. Chen, Phys. Rev. B **93**, 224508 (2016).

[51] K. Kadowaki and S. Woods, Solid State Commun. **58**, 507 (1986).